International Journal of Computer Information Systems and Industrial Management Applications
ISSN 2150-7988 Volume 18(19s) 2026 pp. 47-65
https://doi.org/10.70917/ijcisim-2026-5001
Article

Optimal Bidirectional Power Flow in Probabilistic Solar Conditions Using a Robust Nonlinear Control Approach

Sushama Wankhade[1], Nilima Warke[2], Pankaj Bhirud[3], Manohar Chavan[4]

[1] Assistant Professor, Department of Instrumentation Engineering, Bharati Vidyapeeth College of Engineering, Navi Mumbai, Maharashtra – 400614, India.
Email: sushama.wankhede@bvcoenm.edu.in
[2] Associate Professor, Department of Automation & Robotics, V.E.S. Institute of Technology, Chembur, Mumbai, Maharashtra – 400074, India.
Email: nilima.warke@ves.ac.in
[3] Assistant Professor, Department of Mechanical Engineering, K. V. N. Naik's LoGMIEER, Nashik, Maharashtra, India.
Email: pankaj.bhirud@logmieer.edu.in
[4] Assistant Professor, Department of Automobile Engineering, D. Y. Patil Polytechnic, Ambi, Pune, Maharashtra, India.
Email: m.chavan1985@gmail.com

Abstract: The utilization of solar energy for power stations has gained popularity in recent years. However, due to unpredictable weather conditions and solar irradiance, relying solely on solar energy for power supply throughout the day is not feasible, resulting in an inconsistent power supply to the load. To address the abovementioned issues, this paper addressed by proposing a two-stage grid-connected solar PV system that incorporates an enhanced energy balance control approach that adequately balances the power flow delivery to the load with constant voltage and a properly charged battery. The implementation of the proposed work is evaluated in two stages. Firstly the maximum power point algorithm (MPP) based on POASMC(Perturb& observe adaptive sliding mode control) is used for stochastic solar PV, then integration of an energy storage system with solar PV through a PI controller. Moreover, in the secondary stage, a power flow control logic is proposed and implemented to synchronize solar PV with the grid and analyze the grid-connected PV performance, taking into account the state of charge (SOC) and load current.
Keywords: Photovoltaic systems, Maximum power point technique (MPPT), POASMC, Grid connected system, Hybrid energy storage, Power management,

1. Introduction

The use of technology and industrial equipment has increased dramatically in recent decades; as a result, the demand for energy supply increased rapidly. To fulfil these energy supply demands by coal and fossil fuel-based energy generation system itself creates a negative impact on the environment i.e., global warming, pollution, climate change, and environmental degradation [1] [2]. Therefore, experts and researchers from around the world are investigating alternate energy solutions to address the challenge mentioned above. [3][4].

Renewable energy sources, i.e., in the form of wind energy, solar energy, and geothermal, are gaining popularity as an efficient and viable alternative to traditional energy sources. These energy sources are naturally replenished and do not run out, making them sustainable for energy generation [3]. Among these,wind and geothermal-based energy generators are location-specific and may not be suitable for every location.In contrast,solar energy-based photovoltaic (PV) systems are especially attractive due to their extensive availability, cost-effectiveness, and advanced technology.

However, it is essential to note that PV systems are susceptible to changing environmental circumstances and temperatures, which can affect their efficacy[5] [6][7].

In a solar PV system, when solar insolation changes, the output power of solar PV changes abruptly, impairing solar PV efficiency.To solve this problem,an effective MPPT control algorithm can be used to ensure that solar PV operates at MPP. Many research studies have been conducted to propose different MPPT control algorithms,with perturb & observe (P&O) and incremental conductance (InC) being the most common due to their simplicity and easy understanding [8][9][10]. However, these algorithm techniques for MPP have a few limitations, such as oscillations nearby the peak power and failure to track maximum power due to rapid changes in the environmental conditions. To address these limitations, researchers have designed other controller techniques,including intelligent control techniques [11][12],conventional control techniques [13],sliding mode (SMC) [14], fractional orderSMC [15],swarm-based techniques [16] [6][17], and combination of the controller with optimization techniques [18-21].

Due to the sun's unavailability at night, the irregularity of solar radiation, and the intermittent nature of the PV array, a hybrid renewable energy source with battery storage (PV-BSE) have become necessary for continuous and reliable output power operation. As a result, a renewable energy source with battery storage (PV-BSE) has been developed to provide steady and reliable output power [22]-[25]. Although a limited storage capacity of the battery, it is only possible to provide backup some of the time [26]. Therefore, to obtain continuous power supply at load, if solar energy is not accessible and there are circumstances for energy storing discharge, a grid-connected PV-BES (due to limited availability of grid in the rural area) has been designed and integrated the PV-BES system with a single-phase grid complies with a standard DC bus system [27][7][24]. To maintain the system stability and constant power supply at load with minimum deficiency of power, a power flow management logic has been implemented based on a RESs energy system, battery SOC, and grid current [19][28][29].

Two sub-controllers and one synchronization device have been used for grid-side management. On the grid side, a current controller accurately injects the reference current into the grid through an active/reactive (PQ) controller that is predicated on the necessary P and Q [30] [31]. A phase lock loop (PLL) has been used to synchronize and regulate [32] the grid system with the load demand.The synchronization unit also referred to as the system's center part and is responsible for collecting grid voltage information, i.e., grid frequency, phase, and magnitude.

From the cited literature, it is noticed that there needs to be more research for the situations where there is an adequate power supply from the generation side to meet load demand on the DC bus. So for that situation, mainly when DC load demand is time-varying, and it is integrated with the grid, battery, and renewable energy-based solar PV. To resolve the abovementioned challenges, this article discusses and contributes to a two-stage energy management system based on grid current, battery SOC, and solar power generation. The POASMC MPPT technique is suggested and developed in the first step to get the maximum power energy from PV.The proposed POASMC control approach is further divided into two stages. The initial stage utilizes P&O to generate a reference voltage and control the voltage regulation in an MPPT controller. Furthermore, in the second stage, an upgraded PIDSM controller enforces the solar PV voltage to follow the reference voltage and generates the duty ratio to achieve optimal exploitation of solar PV under varying insolation. The POASMC approach was thoroughly compared with traditional techniques for performance evaluation. Furthermore, for continuous power supply to the load on the DC bus, a PI controller-based energy management strategy for energy distribution based on SOC of battery, power generation of solar and grid current proposed and implemented in the second stage.

The paper presents three significant contributions: Firstly, it introduces the POASMC MPP technique, which is designed and implemented for a grid-connected system capable of handling periodic solar variations in insolation levels from 20 to 1000 W/m2 at 25 ◦C. Secondly; the paper evaluates the efficacy of the suggested POASMC by comparing the output of a 1602 W photovoltaic system with the simulation. Lastly, the authors propose a power flow management algorithm based on renewable energy power generation, battery SOC, and grid current to maintain a constant supply to the load in a stochastic environment. To present the research in a structured manner, the article is divided into different sections. Section 2 describes the general configuration of the proposed system. In Section 3, the paper discusses the DC-DC control, which includes a detailed design description of the boost converter, mathematical modelling of the PV system and MPPT control techniques. Section 4 presents the grid-connected system with a battery and its power flow control algorithm. In Section 5, detailed simulations result and discussion are presented. Finally, the conclusion is shown in the last section.

2. Proposed System Configuration

Figure 1 depicts the typical design of the Solar PV integrated grid charging station used and described in this paper. The design involves using MPPT controller methods with a DC-DC converter to maximize the output of solar PV. To ensure maximum solar PV energy and match the load and source impedance, the boost converter's duty cycle is controlled by a P&O-based sliding mode controller (SMC). The boost converter generates a constant voltageof 350 V for solar PV systems and is connected to a bus system.A DC load, such as a vehicle charging

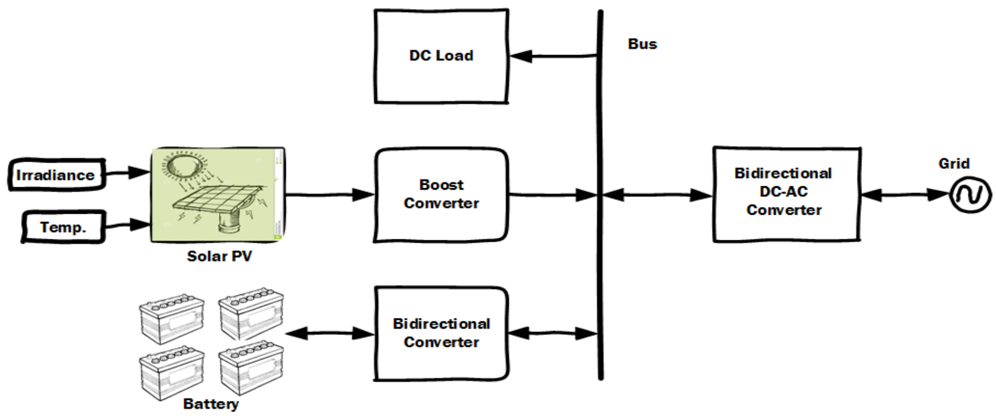

Fig. (1) General architecture of the Solar PV integrated grid charging station

system is connected to the bus system, and a bidirectional converterconnects a battery storage device to the DC bus. Additionally, a bi-directional DC-AC converter that generates anafter-loss 325 V connects the DC bus system to the single-phase grid.

2.1 Solar PV system

Solar PV cells can be modeled for electrical circuit applications using different techniques, with the one-diode module being a popular choice for designing solar PV systems. Equation (1) presents the equation of the solar PV module.

$$I_{total} = I_{Phc} - I_{RSc}\{e^{qed}\frac{(V_{pv}+R_S I_{pv})}{AK_{bc}T} - 1\}\frac{V_{pv}R_S I_{pv}}{R_{sh}} \quad (1)$$

Where,$I_{Phc}$is photodiode current,I_{RSc}reverse saturation current of diode,$e^{qed}$is electron charges, V_{pv},I_{pv}arePVvoltage and current, A denoted as fitting curve factor, R_S,$R_{Sh}$is series and shunt resistance, T istemp. , and K_{bc}valueis taken as$[1.38 * 10^{-23} J/K]$.

It can be inferred from equation (1) that R_{Sh} a solar PV has a ∞value, and the I-V slope curve will be equal to 0 at short circuit conditions. Therefore, in the context of photodiode current, the short circuit current can be substituted by it.

$$I = I_{sc} - I_{RSc}\{e^{qed}\frac{(V_{pv}+R_S I_{pv})}{AK_{bc}T} - 1\} \quad (2)$$

For application specific, the solar PV module written in eq. (2) can be considered as $\left(e^{qed}\,\frac{(V_{pv}+R_sI_{pv})}{AK_{bc}T}\right)$and can be replaced by $\left(e^{qed}\,\frac{(V_{pv}+R_sI_{pv})}{AK_{bc}Tn_s}\right)$, where $n_s$are crystalline solar cells. Therefore, by putting the above values in equation (2), it can be rewritten as:

$$I = I_{sc} - I_{RSc}\{e^{qed}\,\frac{(V_{pv}+R_sI_{pv})}{AK_{bc}Tn_s} - 1\} \quad (3)$$

Rewriting equation (3) as when the PV cell operating in an open circuit, i.e., I=0

$$\frac{e^{qed}}{n_sAK_{bc}T} = \frac{In\left(\frac{I_{SC}}{I_{RSc}}+1\right)}{V_{oc}} \quad (4)$$

Therefore, the solar PV current can be thought of as following equations (3) and (4). $I = I_{sc}\{1 - \frac{I_{Rsc}}{I_{Sc}}(e^{In}(\frac{I_{SC}}{I_{RSc}}+1)\frac{(V_{pv}+R_SI_{pv})}{V_{OC}} - 1\}$ (5)

Taking $z_m = \frac{I_{SC}}{I_{RSc}}$, then equation (5) will be

$$I = I_{SC}\{1 - \frac{1}{z_m}(z_m+1)\frac{(V_{pv}+R_SI_{pv})}{V_{OC}} + \frac{1}{\varsigma}\} \quad (6)$$

Given that the solar PV is considerably bigger than the I_{RSc}, then ς will be high then $\frac{1}{\varsigma}$ is negligible. Therefore, equation (6) will be

$$I = I_{SC}\left(1 - \varsigma\frac{(V_{pv}+R_SI_{pv})}{V_{OC}} - 1\right) \quad (7)$$

2.2 Boost Converter Design

The boost converter in the circuit is utilized to increase the input voltage and act as an interface between the load and the photovoltaic system, especially when there are changes in irradiance and weather conditions. An MPPT control method can be used to modify the boost converter's duty ratio "D," enabling the maximum amount of solar power to be supplied to the load through switch S, ensuring that solar power extraction operates continuously at its highest level of power. The boost converter's performance is expressed in terms of duty cycle "D" [33].

$$P_{Vv}^{\cdot} = \frac{1}{C_{in}}\left[\frac{P_{Vv}}{P_{Vr}} - i_{load}\right]$$

(8)

$$i_{load} = \frac{1}{L}[P_{Vv} - V_O + V_O * D]$$

(9)

Where, i_{load}, $P_{Vv}$are the variable states, D represents the converter duty cycle, V_O is the output voltage, P_{Vr}depicts dynamic resistance,and it can be represented as$P_{Vr} = \frac{\partial P_{Vv}}{\partial P_{Vi}}$.

3. Maximum power point (MPP) algorithm

The main drawback of a commercial Solar PV system is its poor conversion efficiency. As a result, the MPPT algorithm is used to improve system efficiency. Since the MPPT is an essential component of PV systems, the duty cycle regulation is used to manage the Solar PV output. In this regard, to operate solar power at its maximum, a reference voltage uses to generate the required pulses for pulse width modulation (PWM).

A solar photovoltaic (PV) system's efficiency is a crucial aspect, and one of its major drawbacks is its low rate of conversion. To address this issue, MPPT techniques are employed to enhance the efficiency of the system. One of the essential components of a solar PV system is MPPT, and it is regulated by duty cycle control. To ensure that solar power is running at its maximum efficiency, a reference voltage is utilized to generate the required pulses for pulse width modulation (PWM). Therefore, PWM is employed to regulate the output of solar PV systems.

3.1 Incremental conductance (InC) technique

Start

Step-1: Read solar inputs voltage and current$V_{pv}(n)$ and $I_{pv}(n)$

Step-2: Evaluatetotal power$P_{pv}(n) = V_{pv}(n) * I_{pv}(n)$

Step-3: Call P_{pv} and V_{pv}earlier values, i.e.,$P_{pv}(n-1)$ and $V_{pv}(n-1)$

Step-4: Calculate '∂p' and '∂v' using

$\partial v = V_{pv}(n) - V_{pv}(n-1)$ and $\partial p = P_{pv}(n) - P_{pv}(n-1)$

Step-5: If ∂v = 0, Then no change in D and jump to Step 7

Step-6: else If $\partial I > \left[\frac{\partial i}{\partial v} + \frac{1}{v}\right] < \varepsilon$

$\frac{\partial i}{\partial v} > -\frac{1}{v}0$, increase D by $\Delta D$and jump to Step 9.

else decrease the D by ΔD and jump Step 9.

Step-7: If $\left[\frac{\partial i}{\partial v} + \frac{1}{v}\right] < \varepsilon$ then jump toStep 9

Step-8: Else if $\frac{\partial i}{\partial v} > -\frac{1}{v}$, the ΔDincrease and jump to step 9, else ΔD decrease.

Step-9: Calculate $V_{pv}(n)$ and $I_{pv}(n)$

Return.

3.2 Proposed POASMC technique

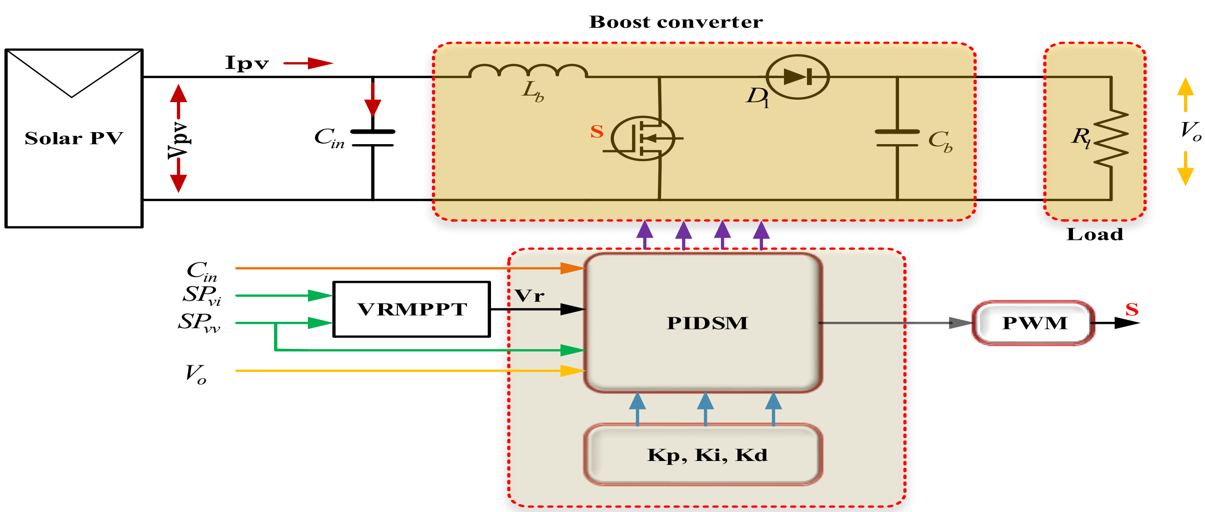

Fig. (2) Block diagram of the Proposed POASMC technique

As previously mentioned in equation (8-9), in boost converter design,a suggested cascade structured PIDSM (PID sliding mode) voltage regulator provides the required D of the signal,driving the boost circuit toward the reference voltage. Therefore, toincreasesolar PV power, PIDSM controller designed using a unique equilibrium-sliding surface by Eq. (10) to improve voltage behaviour of controller.

$$S(t) = K_p e_{rr}(t) + K_D \frac{d}{dt} e_{rr}(t) + K_i \int e_{rr}(t)dt$$

(10)

Where $e_{rr}(t)$ designated asa difference of reference voltage $V_R$and solar voltage$\frac{d}{dt} e_{rr}(t)$, $\int e_{rr}(t)dt$representscorresponding differential and integralerror, andK_p, K_i, $K_D$are controller parameterscoefficient.

The sliding mode control is a composition of identical and discontinuous controller parts and .can be represented as equation (11)

$$C(t) = C_{DIS}(t) + C_{EQ}(t) \quad (11)$$

So, from the above equation (10), to determine the sliding surface of the corresponding control signal, it is formulated and equated to 0. Therefore, equation (10) can be rewritten as

$$S^{\cdot} = K_D e_{rr}^{\cdot\cdot}(t) + e_{ee}^{\cdot}(t) + K_i e_{rr}(t) = 0 \ = -K_D P_{vv}^{\cdot\cdot} - P_{vv}^{\cdot} + K_i e_{rr}(t) = 0 \}$$

(12)

After combining equations(8), (9),and(12), we get

$$\frac{-K_D}{C_{in}}\left[\frac{P_{vv}}{P_{vr}} - i_{load}^{\cdot}\right] - \frac{1}{C_{in}}\left[\frac{P_{vv}}{P_{vr}} - i_{load}^{\cdot}\right] + K_{ierr}(t) = 0 \quad (13)$$

$$\frac{-K_D}{C_{in}}\left(\frac{1}{C_{in}*P_{vr}}\left[\frac{P_{vv}}{P_{vr}} - i_{load}^{\cdot}\right]^{\frown I_{C_1}} - \frac{1}{L}[P_{vv} - V_o + V_o * D]\right) - \frac{1}{C_{in}}\left[\frac{P_{vv}}{P_{vr}} - i_{load}^{\cdot}\right]^{\frown I_{C_1}} + K_{ierr}(t) = 0$$

(14)

Compare equation (14) with equation (11); we can get

$$C_{eq} = \frac{1}{V_o}\left(V_o - P_{vv} + \left(L * I_{C_1}\left[\frac{1}{C_{in}*P_{vr}} + \frac{1}{K_D}\right]\right) - \left[\frac{K_i}{K_D} * L * C_{in} * e_{rr}(t)\right]\right) \quad (15)$$

From equation (11), it can be seen that controller signals are combined with $C_{DIS}(t)$ and $C_{EQ}(t)$. Therefore, the discontinuous $C_{DIS}(t)$ switching of the controller is assumed sigmoidal in this paper to approximate the chattering amplitude as indicated in equation (16).

$$C_{DIS} = -K_d \frac{s}{\|s\| + \varepsilon} \quad (16)$$

where K_d is a small, steady positive integer. After combining equation (15) and equation (16), we obtain equation (17),which shows the overall controller.$C_{EQ} = \frac{1}{V_o}\left(V_o - P_{vv} + \left(L * I_{C_1}\left[\frac{1}{C_{in}*P_{vr}} + \frac{1}{K_D}\right]\right) - \left[\frac{K_i}{K_D} * L * C_{in} * e_{rr}(t)\right]\right) - K_d \frac{s}{\|s\| + \varepsilon}$ (17)

Stability Condition:

$$V = \frac{1}{2} s^2 \quad (18)$$

$$V^{\cdot} = s s^{\cdot} < 0$$

(19)

From equation (8) and (9)

$$P^{\cdot}_{vv} = \frac{1}{C_{in}}\left[\frac{P_{vv}}{P_{vr}} - i_{load}^{\cdot}\right]$$

(20)

$$P^{\cdot\cdot}{}_{vv} = \frac{1}{C_{in}}\left[\frac{P_{vv}{}^{\cdot}}{P_{vr}} - \frac{1}{L}\left[P_{vv} - V_o + V_o * D\right]^{\cdot}\right]$$
(21)

From equation (10)

$$s^{\cdot}(t) = K_D * e^{\cdot\cdot}{}_{rr}(t) + e^{\cdot}{}_{rr}(t) + K_{ierr}(t)$$

$$= K_D * P^{\cdot\cdot}{}_{vv} - P_{vv}{}^{\cdot} + K_{ierr}(t)$$
(22)

Putting equation (20) in (22) and solving

$$s^{\cdot} = \frac{K_D}{{C_{in}}^2 * P_{vr}}\left[\frac{P_{vv}}{P_{vr}} - i_{load}{}^{\cdot}\right] + \frac{K_D}{{C_{in}}^2 * P_{vr}} I_{C_1} + \frac{1}{C_{in}} I_{C_1} - K_{ierr}(t)$$

$$= -\frac{K * K_D * V_o}{L * C_{in}}\left(\frac{s(t)}{\frac{s}{\|s(t)\| + \varepsilon}}\right) - \frac{1}{C_{in}}\left[\frac{P_{vv}}{P_{vr}} - i_{load}{}^{\cdot}\right] + K_{ierr}(t) \quad (23)$$

Where, $I_{C_1} = C_{in}$

$$P_{vv}{}^{\cdot} = \frac{1}{C_{in}}{}^{\cdot}\left[\frac{P_{vv}}{P_{vr}} - i_{load}{}^{\cdot}\right]$$

So equation (23) can be rewritten as

$$s^{\cdot} = -K\left[\frac{K_D * V_o}{L * C_{in}}\right]\overbrace{}^{m} * \frac{s}{\|s\| + \varepsilon} \quad (24)$$

From equation (24) value of m is always positive. So the sign of the equation depends on the sign of K. So, $s^{\cdot}$ considered as

$$s^{\cdot} = -K * \frac{s}{\|s\| + \varepsilon} \quad (25)$$

Putting equation (25) into (19), we can get

$$V^{\cdot} = ss^{\cdot} = \left\{-K\left(\frac{s^2}{\|s\| + \varepsilon}\right)\right\} < 0$$
(26)

$$\left(\frac{s^2}{\|s\| + \varepsilon}\right) > 0$$

$$-K < 0$$

From equation (26), the value of K should be positive for convergence.

4. Power flow control (PFC)

This section covers the power flow controller architecture and logic that controls the operating modes of a grid-tied single-phase inverter. The below flowchart demonstrates the power flow control strategy for maintaining constant voltage in the bus.

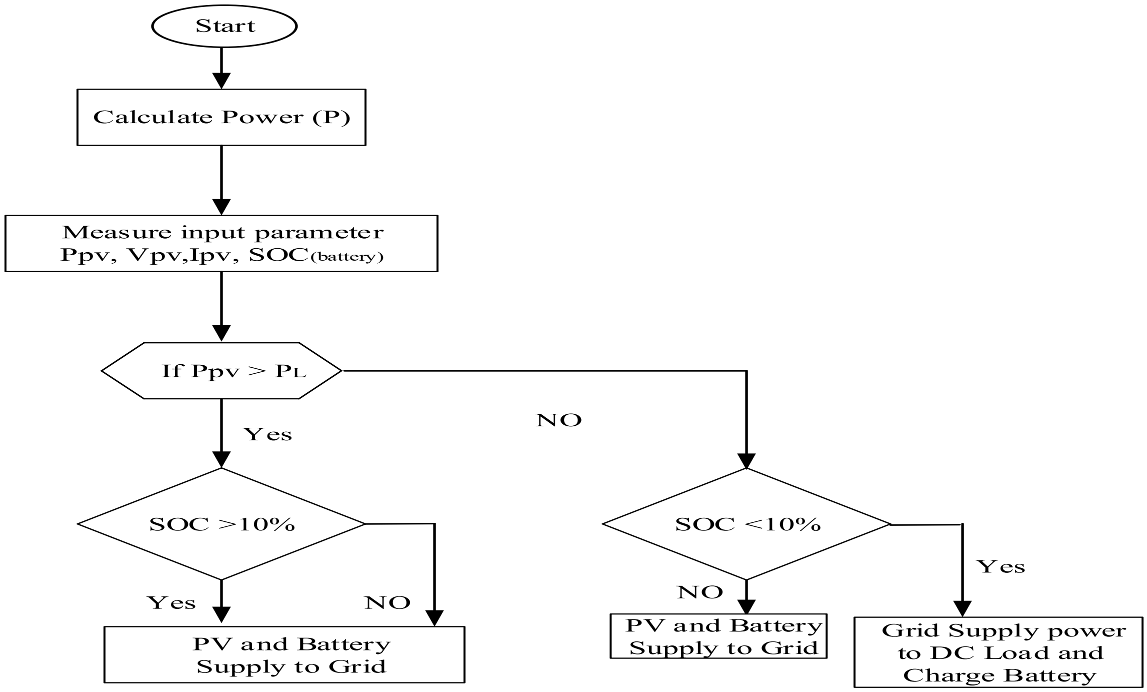

Fig. (3) Control logic for power flow management control

As earlier mentioned, the system operates with a grid-tied single-phase inverter, where the network-determined reference value. Therefore By converting the reference frames of ac waveforms into dc signals, the DQ transformation is used for the reference signal generation. After that, the inverse transform is used to acquire accurate reference signals. The DQ transformation is represented in equation (27) in matrix form, and 'Z' indicates voltage or current.

$$\left[Z_d \, Z_q \right] = \left[sin\, sin\,(\,w_0 t) \;\; -cos\, cos\,(\,w_0 t) \;\; cos\, cos\,(\,w_0 t) \;\; sin\, sin\,(\,w_0 t)\,\right]\left[Z_\alpha \, Z_\beta \right] \tag{27}$$

An imaginary phasor 90 degrees out of phase with reference input is created, enabling DQ transformation. By using Park's transformation method, the DQ frame rotates synchronously with inverter voltage for angular speed as given in equation (28)-(33)

$$\frac{di_{id}}{dt} = \frac{-R_f}{L_f} i_{id} + w_0 i_{qL} + \frac{1}{L_f}(v_{id} - v_{dc}) \tag{28}$$

$$\frac{di_{ql}}{dt} = \frac{-R_f}{L_f} i_{iq} + w_0 i_{dL} + \frac{1}{L_f}(v_{iq} - v_{qc}) \tag{29}$$

$$\frac{dv_{dc}}{dt} = w_0 v_{dc} + \frac{1}{C_f}(i_{id} - i_{dL}) \tag{30}$$

$$\frac{dv_{qc}}{dt} = -w_0 v_{dc} + \frac{1}{C_f}(i_{iq} - i_{qL}) \tag{31}$$

$$\frac{di_{il}}{dt} = \frac{-R_g}{L_g} i_{dL} + w_0 i_{qL} + \frac{1}{L_f}(v_{dc} - v_{dL}) \tag{32}$$

$$\frac{di_{qL}}{dt} = \frac{-R_g}{L_g} i_{gL} + w_0 i_{dL} + \frac{1}{L_f}(v_{qc} - v_{qL}) \tag{33}$$

Now for controlling active and reactive power, equation (34)-(35) used

$$P = v_d i_d + v_q i_q = v_d i_d$$

$$Q = -(v_d i_q + v_q i_d) = -v_d i_q$$

To synchronize the inverter and grid voltage, a phase-locked-loop (PLL) is used. This is accomplished by figuring out the grid current along with the phase angle of the grid voltage. The current controller regulates the grid current Ig using a reference set by the voltage controller. For obtaining the pure sine wave with 350 V amplitude, an LCL filter is used to filter out the harmonics in the inverter output waveform

5. Results and discussion

The research described in this section was carried out using MATLAB Simulink software. The MATLAB Simulink software tool is used for modeling, simulating, and analyzing system dynamics. In the proposed study

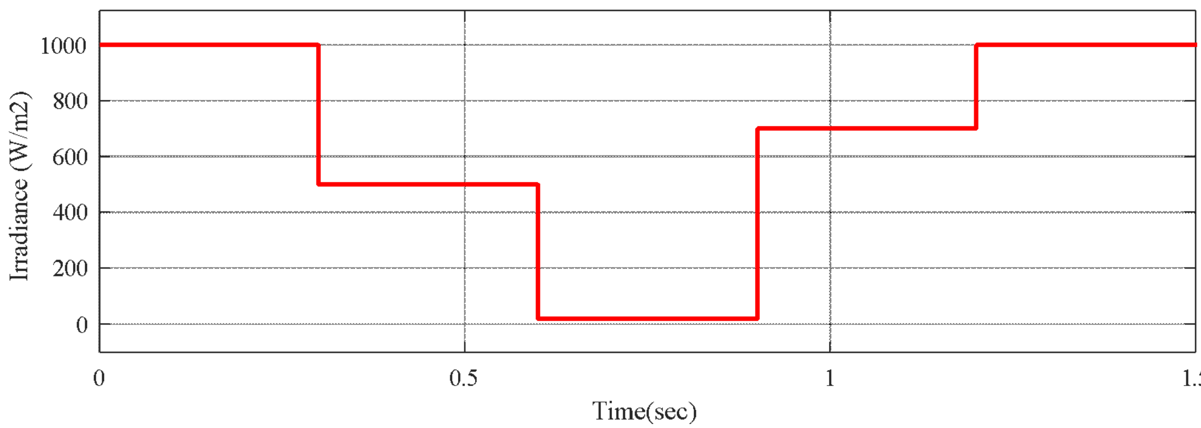

Fig. (4) Solar insolation profile

varied solar insolation profiles in trapezoidal shapes that represent the amount of solar radiation reaching a specific solar region were examined. The solar insulation ranges from 20 to 1000 W/m2 are depicted in Fig (4) and divided into five stages, namely 500, 20, 700, and 1000 W/m2 at a constant temperature, i.e., 25°C. The deviation in solar insulation is considered at 0.3sec, 0.6sec, 0.9sec, and 1.2sec, respectively. Kyocera KC200GT, under standard test scenarios, has been used in this research for solar power generation.

*[Image could not be embedded — unsupported format][Image could not be embedded — unsupported format]*This research aims to look into the performance of the suggested method in response to variations in solar insolation and provide insights into how to improve the efficiency of solar PV output and obtain the maximum possible power from the PV.

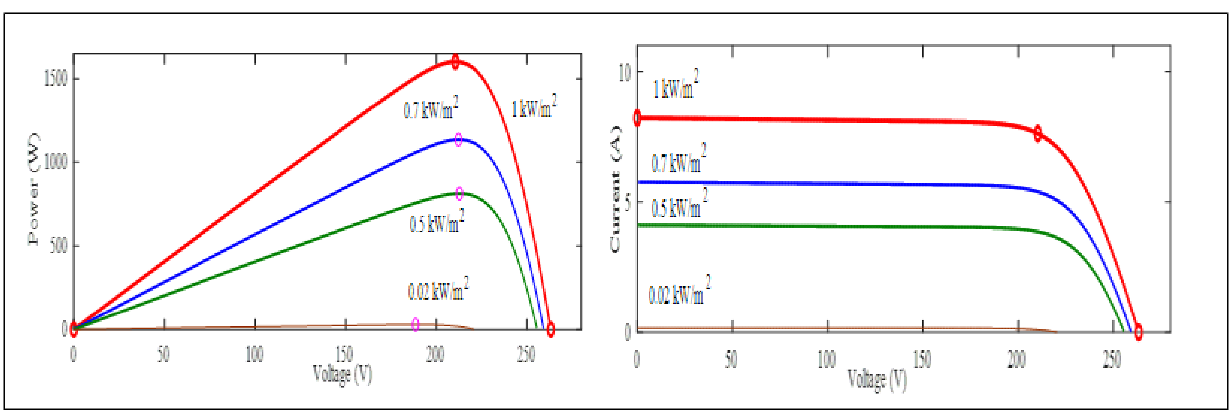

Fig. (5) Solar PV **(a)** PVcharacteristics **(b)** IV characteristics

Figures 5(a) and 5(b) depict the I-V and P-V of the employed Kyocera photovoltaic KC200GT for different temperature and insulation profiles.

In this article, to maximize the power output of a PV array by using three different MPPT techniques: P&O, InC, and POASMC. The performance of these methods was evaluated in both transient and steady-state conditions, under varying climatic conditions, by analyzing the array's voltage, current, and power output. The results are presented in Figures 6(a-c), and a detailed analysis of efficiency, dynamic power output variation, and settling time for each technique is provided in Tables 1 and 2. Overall, the study compares and assesses the effectiveness of these three distinct MPPT approaches.

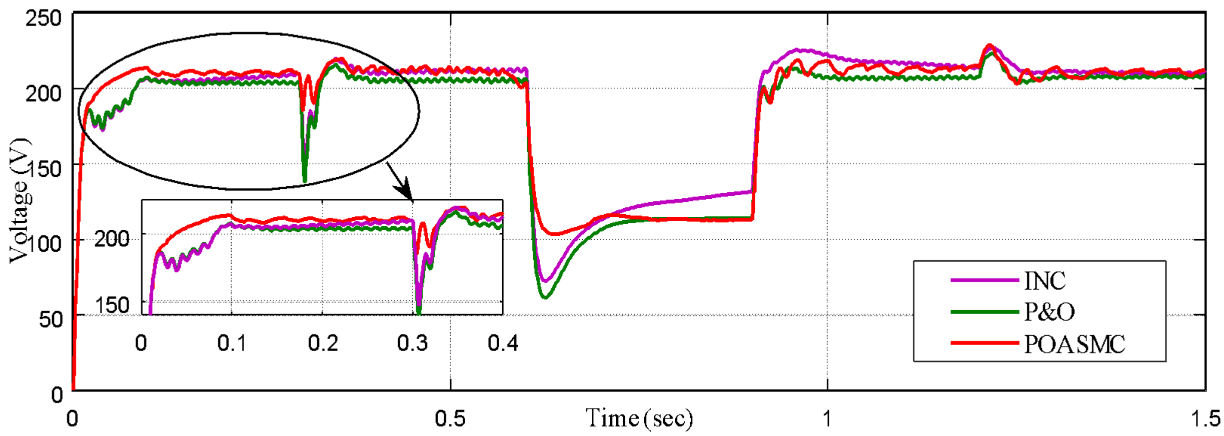

Fig. (6-a) Performance comparison of output voltage

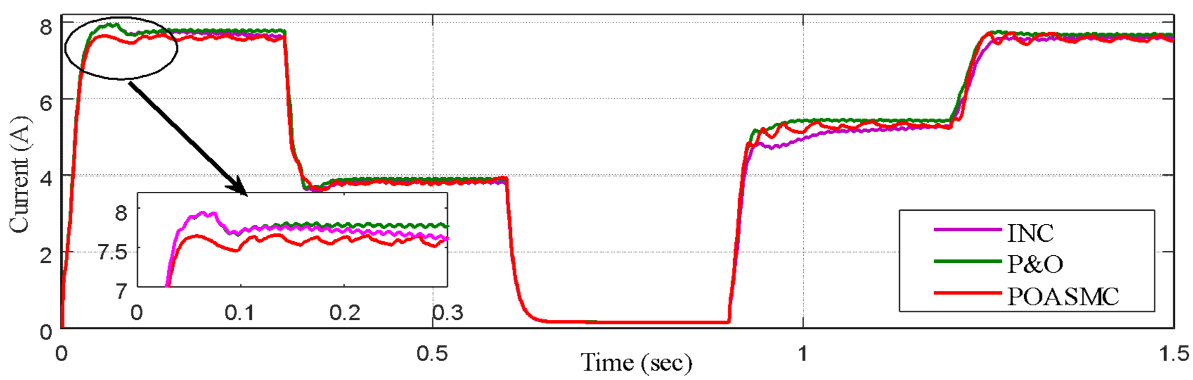

Fig. (6-b) Performance comparison of output current

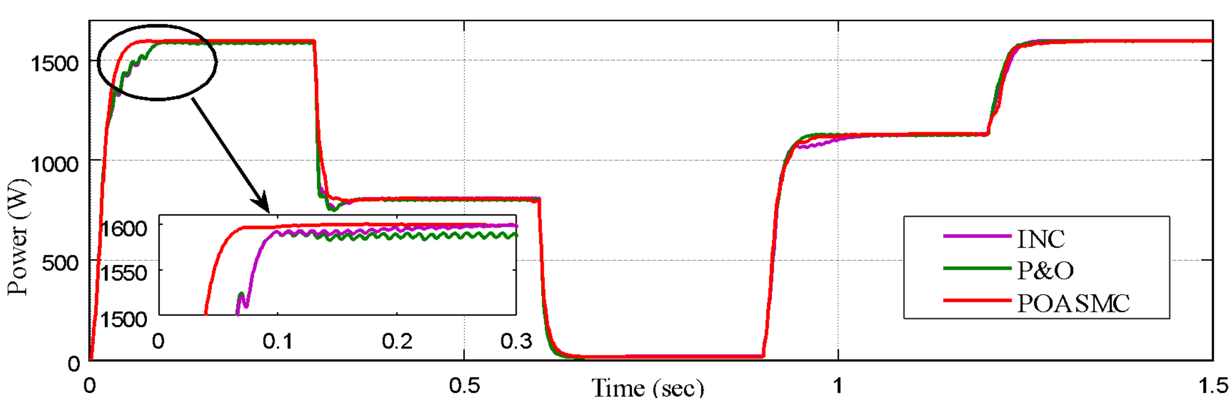

Fig. (6-C) Performance comparison ofoutput power

Table 1: Performance comparison of efficiency for InC, P&O, and proposed POASMC techniques

		Output Power (Achieve)			Efficiency		
Irradiance	Solar output(Ideal)	InC technique	P&O technique	POASMC Proposed	InC technique	P&O technique	POASMC Proposed
20 W/m2	28.83W	19.1W	18W	19.2W	66.25	62.43	66.59
500 W/m2	812W	810W	804W	810W	99.75	99.01	99.75
700 W/m2	1134W	1128W	1128W	1131W	99.47	99.47	99.73
1000 W/m2	1601W	1590W	1586W	1600W	99.31	99.06	99.93

The implemented MPPT method successfully monitors the MPP of solar production in all four studied states, as depicted in Fig. 6(a-c) and Table 1-2. Table 1 shows that the fluctuations near the MPP create a sizable ripple in output power when P&O MPP techniques are employed, as shown in Fig. 6c. As a result, the solar PV array's total output power decreases.Additionally, the use of the InC MPP algorithm results in a significant decrease in ripple content in Ppv. However, this method cannot operate MPP during steady-state conditions. In contrast, the proposed POASMC MPP technique can effectively track the maximum power generated by solar energy with a tracking efficacy of 99.93%, with hardly any ripple content.

Table 2: Performance comparison and analysis ofsettling time and output power variation in InC, P&O, and proposed POASMC techniques

		Output power settling Time			Variation in Output		
Insulation	Solar output (Ideal) Voltage	InC technique	P&O technique	POASMC Proposed	InC technique	P&O technique	POASMC Proposed
1000 W/m2	188.6 V	0.1	0.13	**0.07**	1588-1598W	1584-1590W	1598-1601W
500 W/m2	212.7 V	0.36	0.36	**0.325**	755-810W	770-810W	800-810W
20 W/m2	211.6 V	0.75	0.75	**0.7**	16.6-21.5W	15.2-19.1W	18-19.2W
700 W/m2	210.4 V	1.04	1.05	**0.98**	1124-1128W	1125-1130W	1128-1132W

Furthermore, when comparing the POASMC technique to the P&O and InC techniques for transient performance evaluation, as illustrated in Fig 6 (a-c) and Table(2), the POASMC scheme has a fairly decent response. For achieving maximum solar output when P&O technique used the output responses settling time 0.13sec, 0.36sec, 0.75sec, 1.05sec for 1000 W/m2, 500 W/m2, 20 W/m2 and 700 W/m2 irradiance respectively. Similarly, when the InC technique is used, the settling time for tracking the output power is 0.1sec, 0.36sec, 0.75sec, and 1.04sec, with decreased ripple content in power output for the same irradiance. The PV system employing the POASMC technique shows nearly little ripple content in PV with the minimal settling time of 0.07sec, 0.325sec, 0.7sec, and 0.98sec for 1000 W/m2, 500 W/m2, 20 W/m2, 700 W/m2.

According to the results and extensive research, the suggested POASMC MPPT scheme produces excel results than the P&O and InC approaches in terms of transient and steady-state performance, i.e., more excellent tracking, reduced ripple at the output, and lower settling time. As a result, the suggested POASMC technique has been studied and deployed to track MPP efficiently.

5.1 Grid-connected Solar PV power flow result

A grid-connected solar PV system and battery as storage with inverter operation are discussed in this section. For the combination of 1600W solar PVpower with a single-phase grid, the suggested POASMC MPPT controller's performance has been evaluated regarding grid-side metrics such as the quality of the injected current under periodically changing solar insolation. Variations in solar insolation cause variations in the maximum energy extracted from the solar PV array, as illustrated in Fig. (4). This variation in generated power impacts the constant power supply to the DC bus connected load on battery SOC and the amount of power flow between solar PV and the grid. From Fig 8(c) and 13(c), it can be spotted that Ig (reference current) changes by the change in solar irradiance. So for that, in this article, logic has been designed based on solar PV power and the SOC of the battery in such a way that when solar PV generates access to power, and the SOC of the battery is sufficiently charged generated access power flow in grid side with maintained constant power supply to the load.

Furthermore, if generated power of solar PV is less than the load demand and the SOC of the battery is less than a certain level. The grid provides a power supply to the DC load and charges the battery. To explain this scenario, two conditions have been considered for power flow management.

CASE I: when the SOC of the battery is 50% and the input current is greater than the reference current:

In the first condition, When the SOC of the battery has been considered at 50%, and the solar irradiance is 1000W/m2. In this condition (for 0-0.3sec), solar PV generates 1602W output power. In this scenario, when solar PV produces enough power to keep the DC bus voltage at 350V, then access Solar developed power charges the battery as shown in Fig (7) and Fig (10-b).

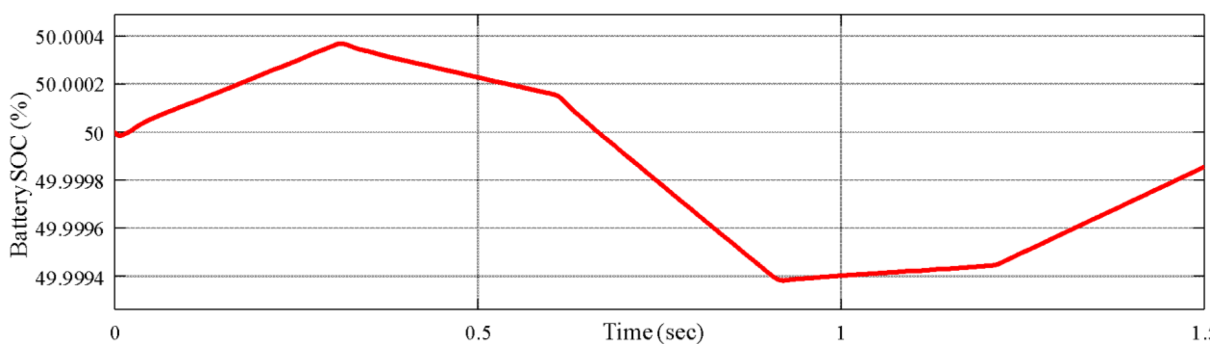

Fig. (7) Battery SOC in case I

It was evident from Fig (10b) that the charging current for the battery is -2 amp. As a result, the 0-0.3sec battery operates in charging mode, and the battery SOC increases. At 0.3 sec, when solar PV irradiance shifts from

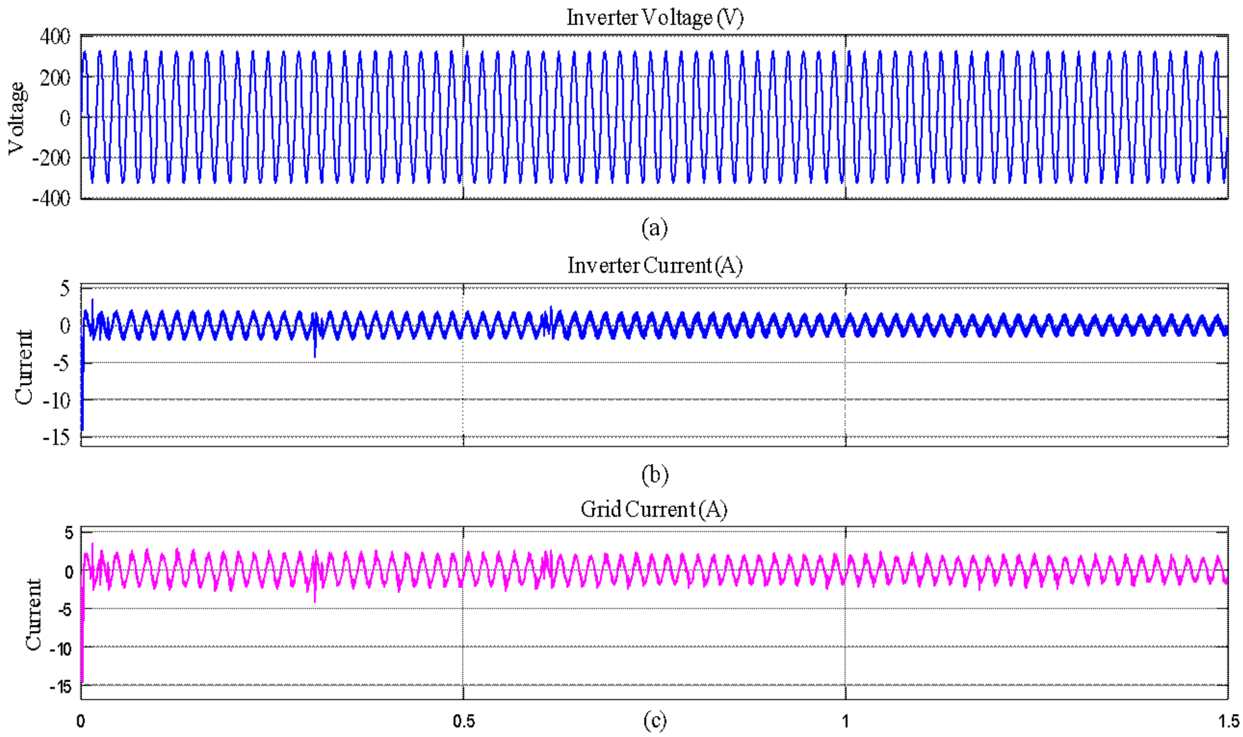

Fig. (8) Case I **(a)** Inverter Voltage (b) Inverter current (c) Grid current

1000w/m2 to 500 w/m2, solar PV generates 812W, as seen in Fig (6c) and Table(1). As shown in Fig (0.3sec-0.6sec), the PV converter current drops from 4A to 2A at this instance (9a). Therefore, to maintain a constant power supply to the DC bus, the battery current switches from negative to positive, and the battery operates in charging to discharging mode to support the continuous power supply to the DC bus, i.e., 350V. Thus, the direction of current movement changes from the solar PV side to the grid side.From 0.6 sec to 0.9 sec, when solar irradiance is 500 w/m2 to 20 w/m2, solar power cannot produce enough (approximately 28 watts) to keep the DC bus voltage constant. As a result, battery-discharging capacity increases to maintain the DC bus voltage constant, as depicted in Fig (10b) and Fig (7). After 0.9 sec, when solar power increases from 28W to 1134W while increasing solar irradiance rises from 20 w/m2 to 700 w/m2, the battery current switches from positive to negative, i.e., discharging to charging mode. In this mode, since solar generates sufficient power to charge the battery and maintain DC bus *[Image could not be embedded — unsupported format]*voltage, the generated access power will flow on the grid side from solar PV.

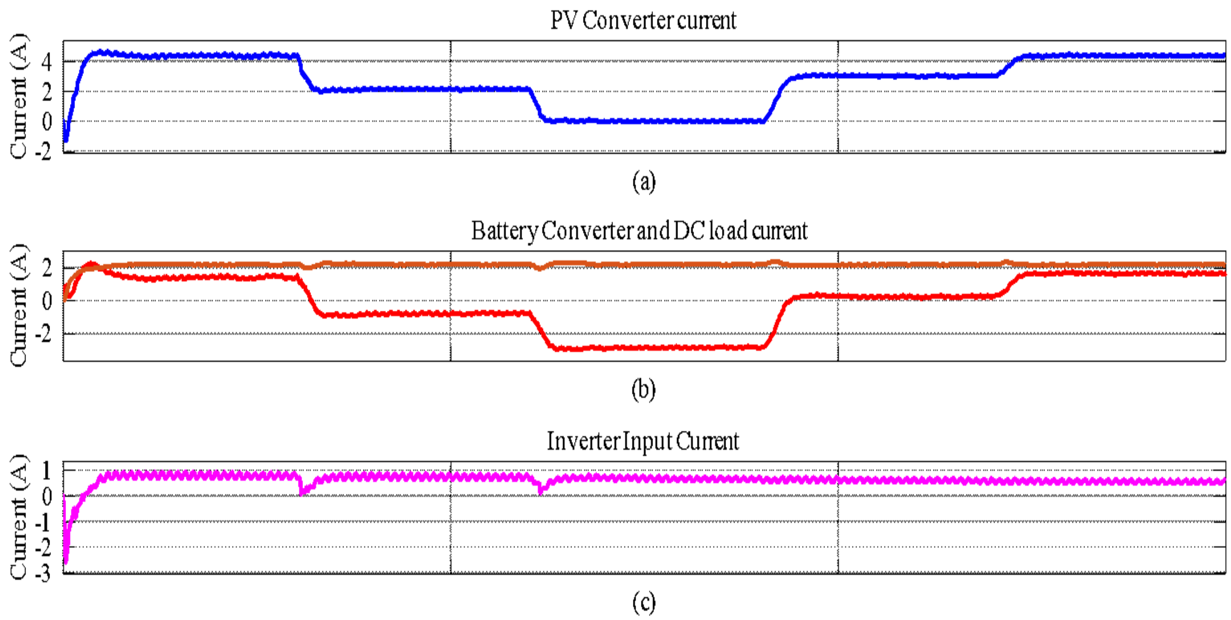

Fig. (9) Case I(a) Solar PV output current (b) Battery converter and load current (c) Input inverter current

Fig (8) shows the inverter voltage, inverter current, and grid current. It is evident from Fig (8) that the grid side

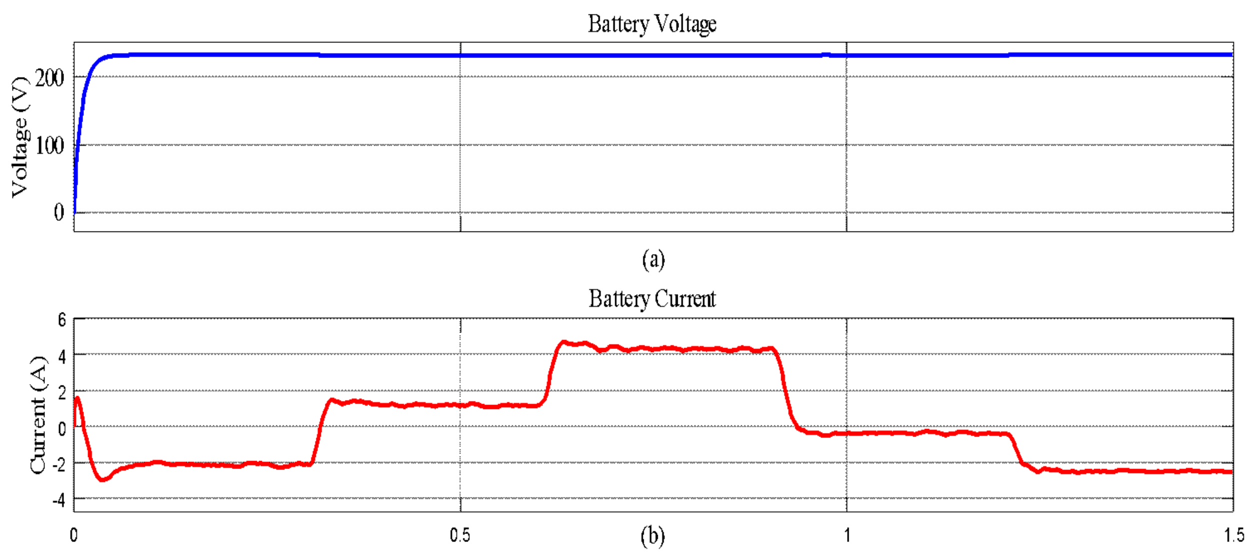

Fig. (10) Case I(a) Battery voltage (b) Battery current

is receiving the accesses power. Thus, the current flow is from solar PV and battery to the grid. Fig (9b) depicts the Battery converter and load current, Fig (9c) inverter input current, Fig (10a) battery voltage, and Fig (11a-c) DC load current, Load voltage, and load power, respectively.

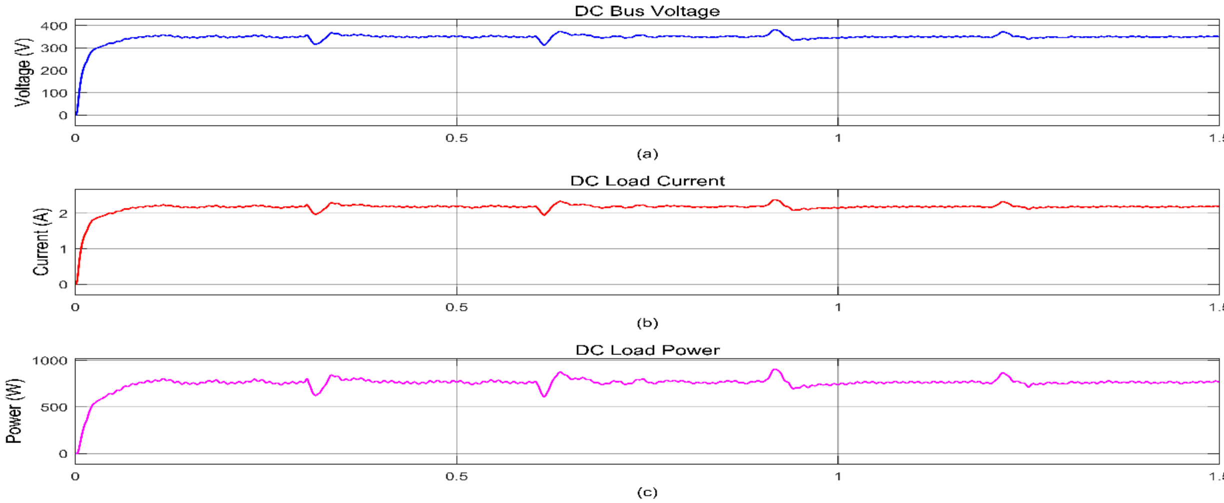

Fig.(11) Case I(a) DC load voltage (b) DC load current (c) DC load power

CASE II: when the SOC of the batteryis less than10%,and the charging current is less than the reference current:

In the second case, when solar irradiance is 1000 w/m2, and the SOC of the battery is less than 10% (i.e., 9.98%). In this condition (0-3sec), solar PV generates 1602W output; it effectively supplies the power to the DC load to maintain bus voltage at 350V. As a result, the battery works in charge mode, as shown in Figures (12) and (14-a).

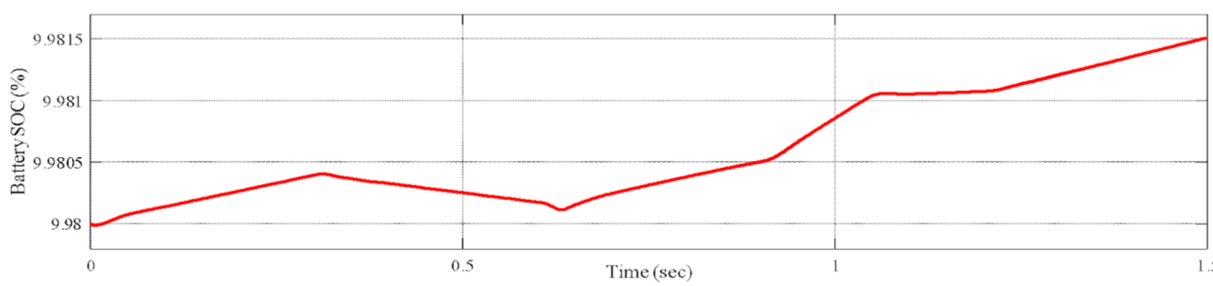

Fig.(12) Battery SOC in case II

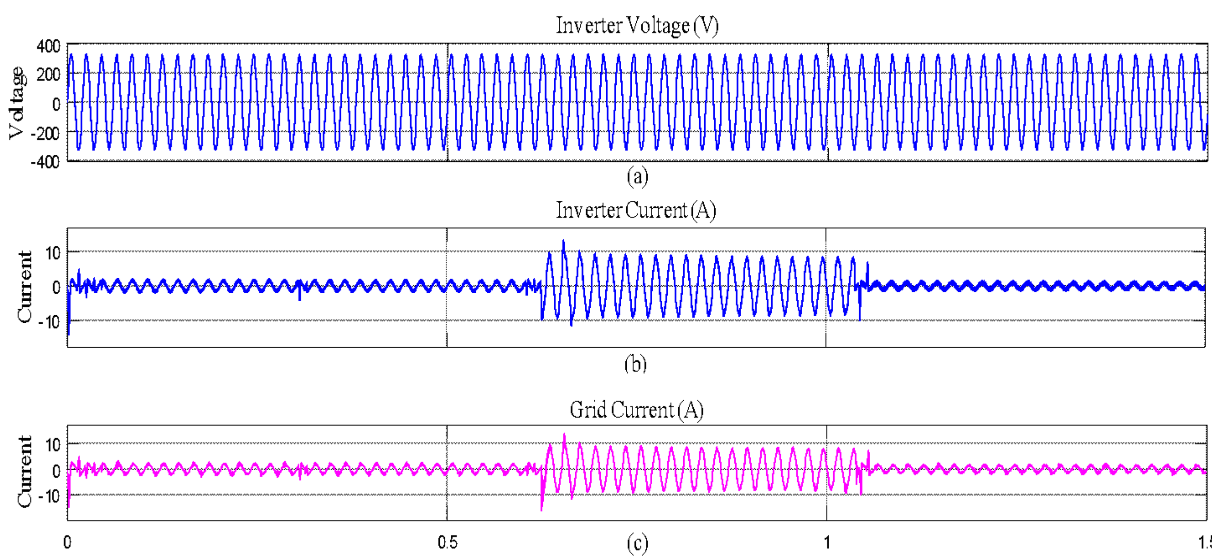

Fig. (13) Case II **(a)** Inverter Voltage (b) Inverter current (c) Grid current

After 0.3 sec to 0.6 sec, when solar irradiance changes from 1000 w/m2 to 500 w/m2, the generated solar output becomes 512 watts. To maintain the DC bus voltage at 350 V, the battery operating mode will change from charging to discharging, as shown in Fig (12). To provide load current efficiently,the battery works in discharging mode. Furthermore, after 0.6sec to 0.9 sec, irradiance falls to 20 w/m2, and solar power generates approx. 28W. In this case, the SOC of the battery is still less than 10%. So, to maintain the DC bus voltage constant, the grid needed to supply power to charge the battery and maintain the DC bus voltage at 350V. After 0.9 sec, when irradiance changes from 20 w/m2 to 700 w/m2, Solar generates 1134W, but battery SOC is still less than 10%. Since the battery SOC is less than the then desired level, it still receives the current from the grid until the battery SOC reaches 9.981%. The power flow in this mode will be from the grid to the solar PV side. It is clearly shown in Fig (13) that when battery SOC is less than 10%, and solar irradiance is 20 w/m2 grid supplies the current to the inverter with 10A.

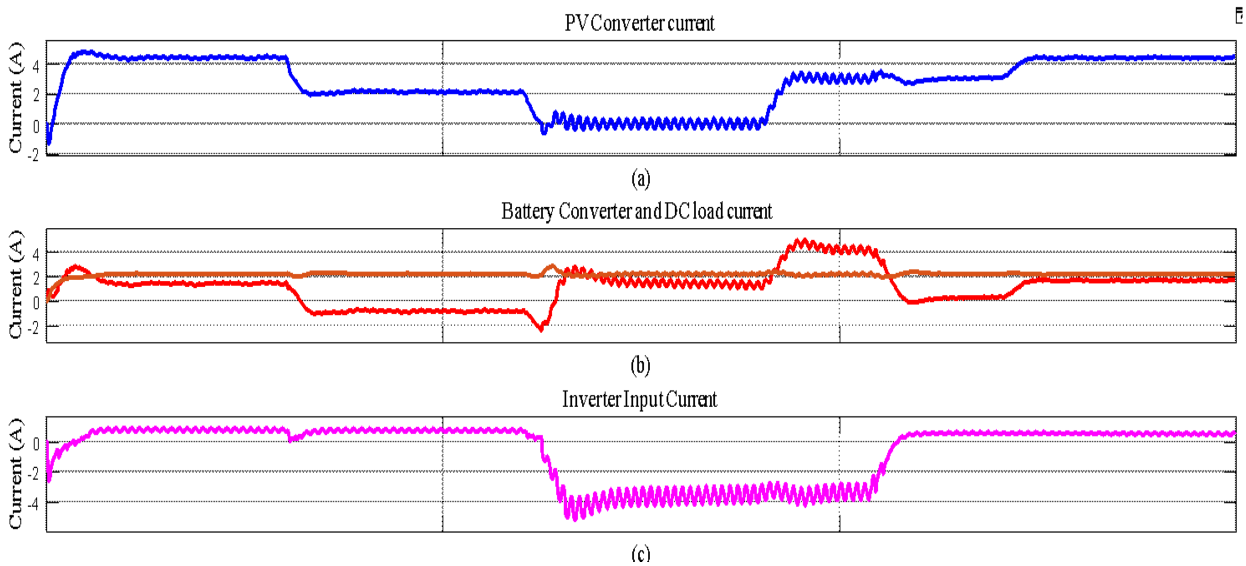

Fig. (14) Case II(a) Solar PV output current (b) Battery converter and load current (c) Input inverter current

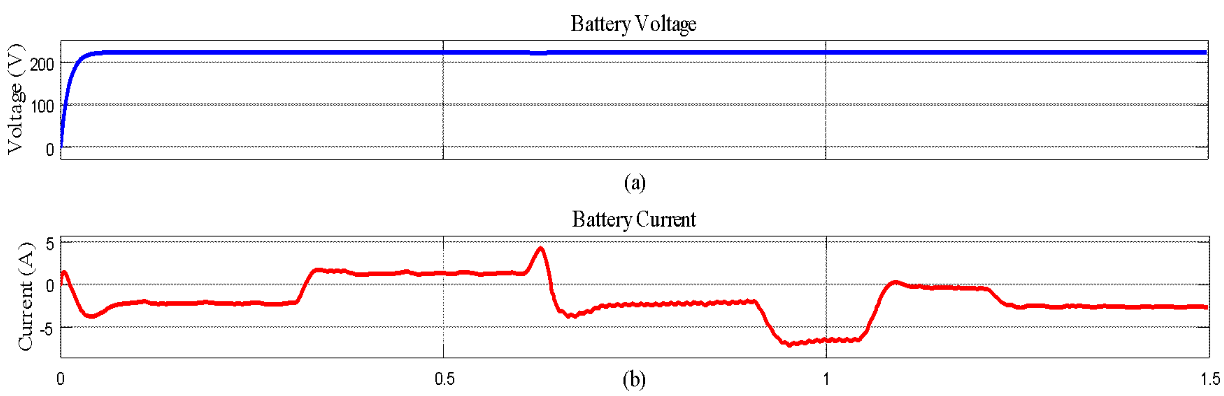

Fig. (15) Case II(a) Battery voltage (b) Battery Current

At 1.2 sec, when solar irradiance changes from 20 w/m2 to 700 w/m2, solar power output becomes, 1602 watts, and battery charging SOC is greater than 9.981%. Then inverter current flow logic changes, solar PV supplies the power to the DC bus load, and the power flow becomes solar PV to the grid side. As a result, the grid and inverter current flow becomes 2A, as shown in Fig (13). Fig (15) and Fig (16) shows the battery voltage, battery current, DC load voltage, load current, and load power, respectively, for different solar irradiance level.

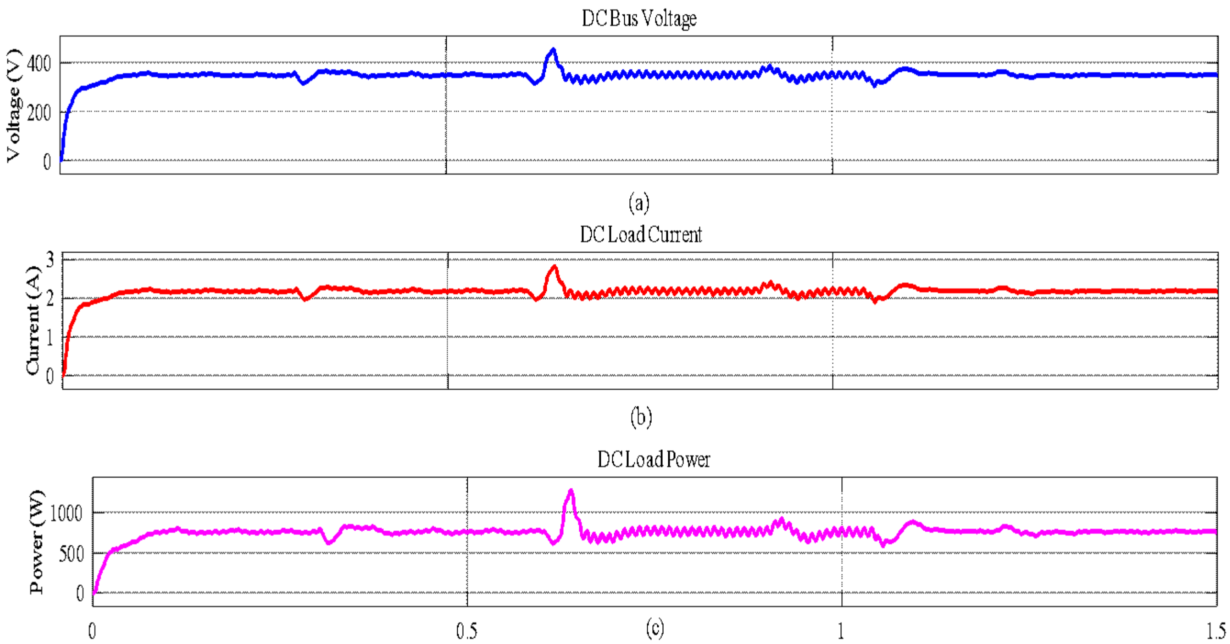

Fig.(16) Case II(a) DC bus voltage (b) DC load current (c) DC load power

6. Conclusion

In conclusion, this article provides a framework for implementing a solar PV, battery, and grid-connected charging station, along with a critical analysis of its performance. The proposed power flow control logic for energy management addresses load demand uncertainty under different solar irradiances. The research highlights the importance of considering the fluctuation of renewable sources and synchronization with the grid system when developing energy management algorithms for renewable energy systems. So for that, two conditions have been considered.First, when the battery's SOC is 50%, and the charging current is greater than the reference current, and second If the battery's SOC is lower than 10% and the charging current lower than the reference current. The PI controller is designed to synchronize solar PV with the grid and battery, while the POASMC MPPT control algorithm is suggested for grid-connected solar PV systems. The study results show that the proposed POASMC MPPT provides improved tracking efficiency with a value of 99.93%, effective faster convergence, with minor deviation from MPP under stochastic solar irradiance compared to traditional P&O and InC. These findings suggest that the proposed framework and techniques can effectively address the challenges of implementing energy management algorithms in renewable energy systems. The research highlights the importance of considering the fluctuation of renewable sources and synchronization with the grid system when developing energy management algorithms for renewable energy systems.

REFERENCES

1. S. Asumadu-Sarkodie and P. A. Owusu, "Carbon dioxide emission, electricity consumption, industrialization, and economic growth nexus: The Beninese case," *Energy Sources, Part B Econ. Plan. Policy*, vol. 11, no. 11, pp. 1089–1096, 2016, doi: 10.1080/15567249.2016.1217286.
2. D. J. Wuebbles and A. K. Jain, "Concerns about climate change and the role of fossil fuel use," *Fuel Process. Technol.*, vol. 71, no. 1–3, pp. 99–119, 2001, doi: 10.1016/S0378-3820(01)00139-4.
3. Wu Y., Wang Z., Huangfu Y, Ravey A., Chrenko D.,Gao F., "Hierarchical Operation of Electric Vehicle Charging Station in Smart Grid Integration Applications — An Overview," *International Journal of Electrical Power & Energy Systems*, vol. 139, no. 108005, 2022, doi: 10.1016/j.ijepes.2022.108005.
4. Rabaia M.K.H, M.A Abdelkareem, Sayed E.T, Elsaid K., Chae J, Wilberforce T, A.G. Olabi, "Environmental impacts of solar energy systems: A review," *Science of The Total Environment.*, vol. 754, no. 141989, 2021, doi: 10.1016/j.scitotenv.2020.141989.

5. Schulz F., Rode J., “Public charging infrastructure and electric vehicles in Norway,” *Energy Policy*, vol. 160, no. Jan, pp. 112660, 2022, doi: 10.1016/j.enpol.2021.112660.
6. Oladepo Olatunde, Mohammad Yusri Hassan, Md Pauzi Abdullah, Hasimah Abdul Rahman,, “Hybrid photovoltaic/small-hydropower microgrid in smart distribution network with grid isolated electric vehicle charging system,” *Journal of Energy Storage*, vol. 31, pp. 101673, 2020, doi: 10.1016/j.est.2020.101673.
7. Talha Hussain Shah, Altamash Shabbir, Adeel Waqas, Abdul Kashif Janjua, Nadia Shahzad, Hina Pervaiz, Sehar Shakir, “The Techno-economic appraisal of electric vehicle charging stations integrated with on-grid photovoltaics on existing fuel stations: A multicity study framework,” *Renewable Energy*, vol. 209, no. 2023, pp. 133–144, 2023, doi: 10.1016/j.renene.2023.03.128.
8. S. Aissani,S.Kahla,M.Bechouat, “A Voltage PID Controller Synthesis Based on a New Small-Signal Linear Model to Enhance the Performance of the Standard P&O Algorithm Employed in Photovoltaic Pannels,” *Arab J Sci Eng*, doi: 10.1007/s13369-022-07494-x.
9. N. Swaminathan and Y. Cao, “An Overview of High-Conversion High-Voltage DC–DC Converters for Electrified Aviation Power Distribution System,” *IEEE Transactions on Transportation Electrification.*, vol. 6, no. 4, pp. 1740–1754, Dec.2020, doi: 10.1109/TTE.2020.3009152.
10. Kok Soon Tey, Saad Mekhilef, , “Modified incremental conductance MPPT algorithm to mitigate inaccurate responses under fast-changing solar irradiation level,” *Solar Energy*, vol. 101, pp. 333–342, 2014, doi: 10.1016/j.solener.2014.01.003.
11. P. K. Pathak AK Yadav, P Sanjeevikumar, PA Alvi, “Design of robust multi-rating battery charger for charging station of electric vehicles via solar PV system,” *Electric Power Components and Systems*, vol. 50, no. 14-15,, pp. 751–761, 2022, doi: 10.1080/15325008.2022.2139870.
12. S. Tripathi, A. Shrivastava, K. C. Jana, S. Tiwari, V. S. Bhadoria, and Anurag, “Fuzzy logic controller based solar MPPT and battery charging for hybrid vehicle application,” *AIP Conf. Proc.*, vol. 2294, no. December, 2020, doi: 10.1063/5.0031840.
13. Lins, A.W., Krishnakumar, R., “Tuning of PID controller for a PV-fed BLDC motor using PSO and TLBO algorithm,” *Appl Nanosci.*, vol. 13,pp. 2911-2933, 2023, doi: 10.1007/s13204-021-02272-x.
14. Huang S., Wang Jie, Huang C., Zhou L.,Xiong L, Liu J., Li P., "A fixed-time fractional-order sliding mode control strategy for power quality enhancement of PMSG wind turbine,” *International Journal of Electrical Power & Energy Systems.*, vol. 134, pp. 107354, 2022, doi: 10.1016/j.ijepes.2021.107354. [15] Lau J.Y., Liang W., Tan K.K, “Adaptive sliding mode enhanced disturbance observer-based control of surgical device,” *ISA Transactions*, vol. 90, p. 178-188, 2019, doi: 10.1016/j.isatra.2018.12.048.
15. A. Goswami and P. Kumar Sadhu, “Stochastic firefly algorithm enabled fast charging of solar hybrid electric vehicles,” *Ain Shams Eng. J.*, vol. 12, no. 1, pp. 529–539, 2021, doi: 10.1016/j.asej.2020.08.016.
16. A. Awasthi, K. Venkitusamy, S. Padmanaban, R. Selvamuthukumaran, F. Blaabjerg, and A. K. Singh, “Optimal planning of electric vehicle charging station at the distribution system using hybrid optimization algorithm,” *Energy*, vol. 133, pp. 70–78, 2017, doi: 10.1016/j.energy.2017.05.094.
17. S. Tripathi, A. Shrivastava, and K. C. Jana, “Self-Tuning fuzzy controller for sun-tracker system using Gray Wolf Optimization (GWO) technique,” *ISA Trans.*, vol. 101, pp. 50–59, 2020, doi: 10.1016/j.isatra.2020.01.012.
18. S. Singh, P. Chauhan, and N. J. Singh, “Capacity optimization of grid connected solar/fuel cell energy system using hybrid ABC-PSO algorithm,” *Int. J. Hydrogen Energy*, vol. 45, no. 16, pp. 10070–10088, 2020, doi: 10.1016/j.ijhydene.2020.02.018.
19. S. A. Gorji, H. G. Sahebi, M. Ektesabi, and A. B. Rad, “Topologies and control schemes of bidirectional DC–DC power converters: An overview,” *IEEE Access*, vol. 7, pp. 117997–118019, 2019, doi: 10.1109/ACCESS.2019.2937239.
20. D.Sakthivel, S.S., Arunachalam, V. Artificial Neural Network Assisted P &O-Based MPPT Controller for a Partially Shaded Grid-Connected Solar PV Panel. ,” *Arab J Sci Eng (2022)*, doi: 10.1007/s13369-022-07566-y.
21. A. K. Karmaker, M. R. Ahmed, M. A. Hossain, and M. M. Sikder, “Feasibility assessment & design of hybrid renewable energy based electric vehicle charging station in Bangladesh,” *Sustain. Cities Soc.*, vol. 39, pp. 189–202, 2018, doi: 10.1016/j.scs.2018.02.035.
22. L. S. A. Grande, I. Yahyaoui, and S. A. Gómez, “Energetic, economic and environmental viability of off-grid PV-BESS for charging electric vehicles: Case study of Spain,” *Sustain. Cities Soc.*, vol. 37, no. November 2017, pp. 519–529, 2018, doi: 10.1016/j.scs.2017.12.009.
23. J. A. Domínguez-Navarro, R. Dufo-López, J. M. Yusta-Loyo, J. S. Artal-Sevil, and J. L. Bernal-Agustín, “Design of an electric vehicle fast-charging station with integration of renewable energy and storage systems,” *Int. J. Electr. Power Energy Syst.*, vol. 105, no. March 2018, pp. 46–58, 2019, doi: 10.1016/j.ijepes.2018.08.001.
24. D. Yan, H. Yin, T. Li, and C. Ma, “A Two-Stage Scheme for Both Power Allocation and EV Charging Coordination in a Grid-Tied PV-Battery Charging Station,” *IEEE Trans. Ind. Informatics*, vol. 17, no. 10, pp. 6994–7003, 2021, doi: 10.1109/TII.2021.3054417.
25. S. Chtita, A. Derouich, A. El Ghzizal, and S. Motahhir, “An improved control strategy for charging solar batteries in off-grid photovoltaic systems,” *Sol. Energy*, vol. 220, no. October 2020, pp. 927–941, 2021, doi: 10.1016/j.solener.2021.04.003.

26. P. Prem, P. Sivaraman, J. S. Sakthi Suriya Raj, M. Jagabar Sathik, and D. Almakhles, “Fast charging converter and control algorithm for solar PV battery and electrical grid integrated electric vehicle charging station,” *Automatika*, vol. 61, no. 4, pp. 614–625, 2020, doi: 10.1080/00051144.2020.1810506.
27. V. Karthikeyan and R. Gupta, “Multiple-Input Configuration of Isolated Bidirectional DC-DC Converter for Power Flow Control in Combinational Battery Storage,” *IEEE Trans. Ind. Informatics*, vol. 14, no. 1, pp. 2–11, 2018, doi: 10.1109/TII.2017.2707106.
28. K. L. Lopez, C. Gagne, and M. A. Gardner, “Demand-side management using deep learning for smart charging of electric vehicles,” *IEEE Trans. Smart Grid*, vol. 10, no. 3, pp. 2683–2691, 2019, doi: 10.1109/TSG.2018.2808247.
29. M. M. Mahfouz and M. R. Iravani, “Grid-Integration of Battery-Enabled DC Fast Charging Station for Electric Vehicles,” *IEEE Trans. Energy Convers.*, vol. 35, no. 1, pp. 375–385, 2020, doi: 10.1109/TEC.2019.2945293.
30. L. Hassaine and M. R. Bengourina, “Control technique for single phase inverter photovoltaic system connected to the grid,” *Energy Reports*, vol. 6, no. September 2019, pp. 200–208, 2020, doi: 10.1016/j.egyr.2019.10.038.
31. K. Saleem, Z. Ali, and K. Mehran, “A Single-Phase Synchronization Technique for Grid-Connected Energy Storage System under Faulty Grid Conditions,” *IEEE Trans. Power Electron.*, vol. 36, no. 10, pp. 12019–12032, 2021, doi: 10.1109/TPEL.2021.3071418.
32. Van Dijk E, Spruijt JN, O’sullivan DM, Klaassens JB. PWM-switch modelling ofDC-DC converters. IEEE Trans Power Electron 1995;10(6):659–65